

The phonon dispersion of graphite by inelastic x-ray scattering

M. Mohr,^{1,*} J. Maultzsch,^{1,†} E. Dobardžić,² S. Reich,³ I. Milošević,²

M. Damnjanović,² A. Bosak,⁴ M. Krisch,⁴ and C. Thomsen¹

¹*Institut für Festkörperphysik, Technische Universität Berlin, Hardenbergstr. 36, 10623 Berlin, Germany*

²*Faculty of Physics, University of Belgrade, POB 368, 11011 Belgrade, Serbia*

³*Department of Materials Science and Engineering, Massachusetts Institute of Technology, 77 Massachusetts Avenue, Cambridge, MA 02139-4307, USA*

⁴*European Synchrotron Radiation Facility (ESRF), BP 220, F-38043 Grenoble cedex, France*

(Dated: February 8, 2022)

We present the full in-plane phonon dispersion of graphite obtained from inelastic x-ray scattering, including the optical and acoustic branches, as well as the mid-frequency range between the K and M points in the Brillouin zone, where experimental data have been unavailable so far. The existence of a Kohn anomaly at the K point is further supported. We fit a fifth-nearest neighbour force-constants model to the experimental data, making improved force-constants calculations of the phonon dispersion in both graphite and carbon nanotubes available.

PACS numbers: 63.20.Dj, 63.70.+h, 78.70.Ck

I. INTRODUCTION

Research on carbon nanotubes and the recent availability of single graphite sheets^{1,2} (graphene) has revived the interest in the fundamental physical properties of graphite during the last years. Carbon nanotubes can be regarded as one or more rolled-up graphite sheets, and many physical properties of carbon nanotubes are closely related to those of graphite.^{3,4}

The fundamental characteristics of a crystalline material comprise its phonon spectrum, from which one can derive several other physical properties such as sound velocity, thermal conductivity, or heat capacity. Furthermore, phonons play an important role in excited-state dynamics and electrical transport properties. Optical or electronic excitations can decay into vibrational excitations or can be scattered by phonons into different states. For example, in carbon nanotubes the high-bias electrical transport is assumed to be limited by scattering of the carriers by optical phonons corresponding to the graphite K point.^{5,6}

The phonon dispersion of graphite has not been completely resolved by experiment, mostly due to the lack of large enough samples of crystalline quality. It has been partly measured by inelastic neutron scattering (INS), electron-energy loss spectroscopy (EELS), and inelastic x-ray scattering (IXS).^{7,8,9,10,11} Most experiments so far have determined the dispersion along the $\Gamma - K$ and the $\Gamma - M$ directions in the graphite Brillouin zone (see Fig. 1 for a definition of the Brillouin zone). The recent measurement of the optical branches along the $K - M$ direction by IXS pointed to the existence of a Kohn anomaly for the highest phonon branch at the K point.^{11,12} Although this result resolved previous discrepancies between different lattice dynamics models, there are still open questions regarding the shape of lower-lying phonon branches. In particular, differences appear between force-constants and density-functional theory (DFT) calculations, where experimental data are still unavailable. This concerns, e.g., the crossing between the acoustic and optical bands near the M -point or the energy of the transverse acoustic mode at the K point. For carbon nanotubes, the experimen-

tal determination of the phonon dispersion throughout the entire Brillouin zone would require monocrystalline samples of a minimum size, which have been unavailable so far. Therefore, the closest approximation to the experimental phonon dispersion of carbon nanotubes is currently the phonon dispersion of graphite.

Here we present the phonon dispersion of graphite in all three high-symmetry directions in the basal plane determined by inelastic x-ray scattering. In particular, the phonon branches between the K and M point and the acoustic branches in all high-symmetry directions are obtained, giving both the optical and acoustic phonons from one experimental technique. We fit our data by a set of force constants, including fifth-nearest neighbours of carbon atoms. The fitted force constants can be used to deduce the corresponding force constants for carbon nanotubes.

This paper is organized as follows. In the next section we briefly describe the experimental details of the IXS experiments. We give an introduction to the phonon dispersion of graphite and present the experimental data in Sect. III. In Sect. IV we apply a fifth-nearest neighbour force constants fit to the experimental data and provide the in-plane and out-of-plane force constants.

II. EXPERIMENTAL SETUP

The inelastic x-ray experiments were performed at beam line ID28 at the European Synchrotron Radiation Facility (ESRF). For a review of IXS the reader is referred to Refs. 13 and 14. The energy of the incident radiation of 17794 eV was selected by the (999) Bragg reflection of a silicon crystal. The scattered photons were analyzed by five analyzers operating in the same reflection order. The total energy resolution in this configuration is 3.0 meV.¹⁴ The x-ray beam was focused to $250 \times 60 \mu\text{m}^2$, selecting a single microcrystal in a naturally grown graphite flake. The typical size of a single grain was about $800 \mu\text{m}$ in lateral direction and $100 \mu\text{m}$ along the c -axis. By x-ray diffraction we obtained the lattice

parameters $a = 2.463 \text{ \AA}$ and $c = 6.712 \text{ \AA}$, in excellent agreement with previous neutron diffraction data ($a = 2.464 \text{ \AA}$, $c = 6.711 \text{ \AA}$).¹⁵

Inelastic scattering spectra were recorded by varying the temperature difference between the monochromator and the analyzer silicon crystal. To minimize the effects of temperature drifts that could result in an energy offset, we performed systematic Stokes–anti-Stokes scans between the measurements. In our setup the c -axis of graphite and the scattering plane encompasses an angle of 90° , 30° , and 0° , depending on the phonon branch under consideration. The scattering geometry was chosen according to the selection rules, see Ref. 16.

III. EXPERIMENTAL RESULTS

The unit cell of graphene contains two atoms, resulting in six phonon branches. The unit cell of graphite consists of four atoms, which leads to twelve phonon branches. The space group of graphite is $P6_3/mmc$ (international notation). At the Γ point it possesses the factor group $6/mmm$ (D_{6h} in Schönflies notation). The optical zone-center modes of graphene are decomposed into $\Gamma = B_{2g} + E_{2g}$. In graphite, the optical zone center modes are decomposed into $\Gamma = A_{2u} + 2B_{2g} + E_{1u} + 2E_{2g}$.^{17,18,19} The A_{2u} and E_{1u} modes are IR active, the E_{2g} modes Raman active. The B_{2g} modes are optically inactive, but can be measured via INS or IXS. The three acoustic modes are decomposed into $\Gamma = A_{2u} + E_{1u}$.

Graphite is a highly anisotropic material: the nearest-neighbor distance between two atoms in the plane is $a/\sqrt{3} \approx 1.42 \text{ \AA}$, while the inter-layer distance is $c/2 \approx 3.35 \text{ \AA}$. The bonds between two carbon atoms in the plane are much stronger than the weak van-der-Waals interactions between the layers. Therefore, compared to graphene, one expects that the phonon modes of graphite correspond approximately to in-phase and out-of-phase vibrations of the two graphene planes. Most of the phonon branches in graphite are nearly doubly degenerate and almost the same as in graphene.^{12,20} Only close to the Γ point, the acoustic modes of the single layer split in graphite into an acoustic mode (in-phase vibration of the graphene sheets) and an optical mode [out-of-phase vibration; in-plane: E_{2g} at 5.2 meV (42 cm^{-1}); out-of-plane: B_{2g} at 15.7 meV (127 cm^{-1})]. For the optical modes of graphite, the difference between the in-phase and the out-of-phase vibrations is very small: at the Γ point the IR active E_{1u} mode is found at 196.9 meV (1588 cm^{-1}), close to the Raman active E_{2g} mode at 196.0 meV (1581 cm^{-1}). The same holds for the A_{2u} mode at 107.5 meV (867 cm^{-1})^{17,21} and the B_{2g} mode at 107.6 meV (868 cm^{-1}). Therefore, in the following theoretical discussion, we will consider the phonons of a single graphene sheet.

The six branches are divided into the out-of-plane acoustic mode ZA, the in-plane acoustic mode TA (sometimes called SH=shear), the longitudinal acoustic mode LA, the out-of-plane optical mode ZO, the in-plane optical mode TO (SH*), and the longitudinal optical mode LO. Four branches belong to modes where the atoms move in-plane with the graphene layer (TA, LA, TO, LO); two branches belong to transverse

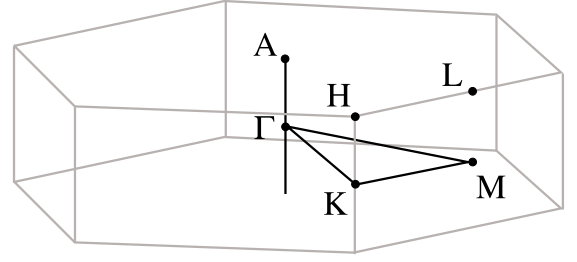


FIG. 1: Brillouin zone of graphite. The Brillouin zone of graphene is the hexagon which lies in the plane with the points Γ , K and M . The distances between the high-symmetry points are $\Gamma - K = 4\pi/3a$, $\Gamma - M = 2\pi/\sqrt{3}a$, and $K - M = 2\pi/3a$.

modes, where the atoms move out of the plane (ZA, ZO).

In Fig. 2 we show our experimental data of the graphite phonon dispersion in the plane. The lines show the fifth-nearest neighbor force-constants fit described in Sect. IV. The optical phonon frequencies near the Γ point agree well with previous experiments. We find the E_{2g} LO mode at 196.0 meV (1581 cm^{-1}), and the B_{2g} mode at 107.6 meV (868 cm^{-1}). Regarding the overall shape of the phonon branches, our experiments confirm previous *ab-initio* DFT calculations, letting aside the special situation for the highest branch at the K point.^{11,12,20,22,23}

As can be seen, the highest optical frequency does not appear at the Γ -point. Instead, the phonon frequency first increases with larger wave vector and then decreases again. This effect, called overbending, has been observed in diamond as well.²⁴ In graphite, it has been predicted to result from a Kohn anomaly, i.e., the frequency at the Γ point is lowered due to interaction of the phonon with the electronic system.^{11,12} Another Kohn anomaly in graphite can be found for the TO-derived phonon branch at the K -point (fully symmetric A'_1 (K_1) mode). We have gained additional data for the highest optical phonons around the K point, confirming previous measurements of the frequency softening of the TO-derived branch near the K point.¹¹ Again, we were not able to detect the A'_1 phonon directly at the K point. The strong electron-phonon interaction has been predicted to reduce the phonon lifetime which results in a line broadening. Probably the large line width makes it very difficult to detect the A'_1 phonon at the K point experimentally.

Considering the differences between previous theoretical models, we find the following results, see also Sect. IV. Between the Γ and M points, the ZO and TA modes do not cross within our experimental error of 3 meV . This is in contrast to previous empirical force-constants models and EELS data of Ref. 8. Which branch is higher directly at the M point cannot be uniquely distinguished from our data. However, in DFT phonon calculations the crossing is found between K and M but close to M (about $1/10$ of the distance between K and M , see Ref. 23). The overall agreement with DFT calculations supports the crossing between K and M , see also Fig. 3.

The TA branch along $\Gamma - M$ shows a smaller increase compared to the electron energy loss spectroscopy (EELS) data in Ref. 8. In a recent EELS experiment on epitaxially grown thin

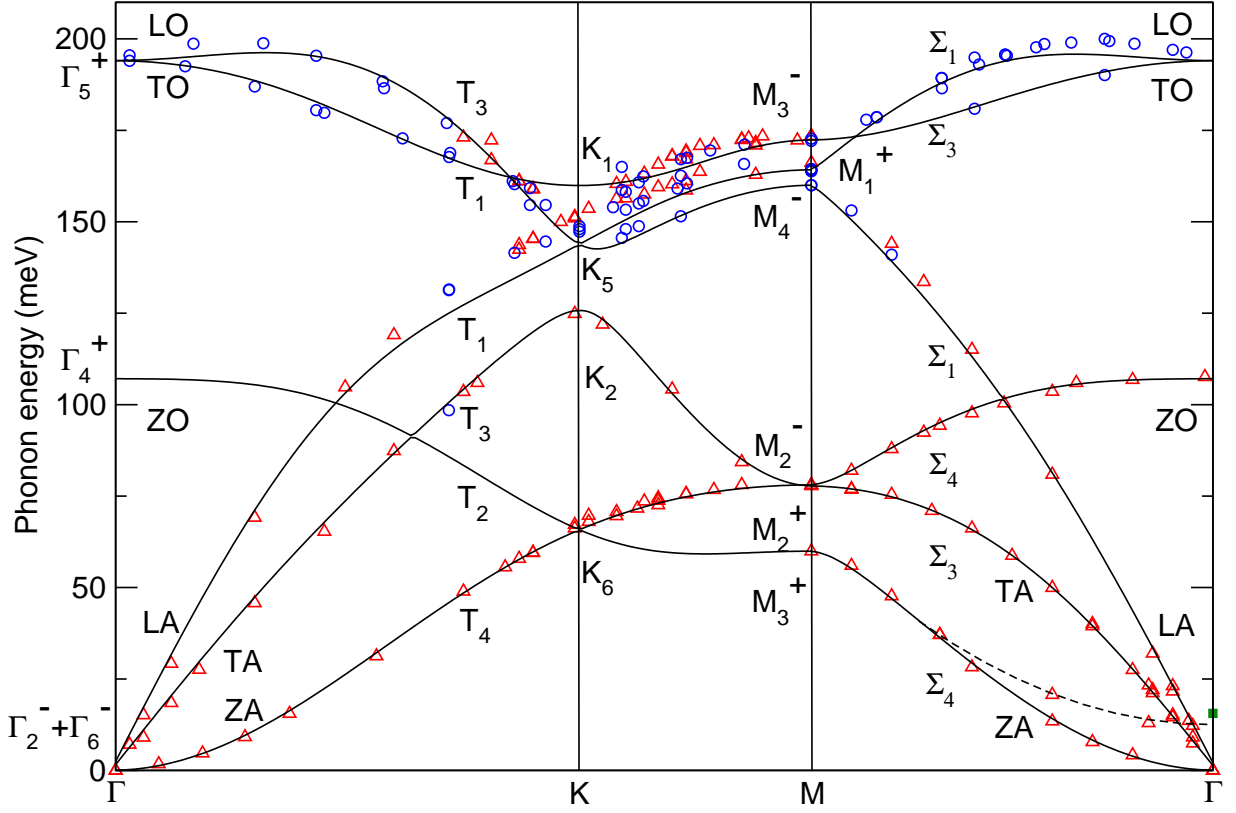


FIG. 2: (Color online) Phonon dispersion of graphite from inelastic x-ray scattering (symbols). Triangles are present data, circles are data already published in Ref. 11. The full square at the Γ point is INS data from Ref. 7. Solid lines are the force-constants calculations from the 5th-nearest neighbor fit discussed in Sect. IV; the dashed line is a quadratic extrapolation of the data. The lines are denoted by their symmetry representation in space group notation. The relation between space group and molecular notation can be found in Table I.

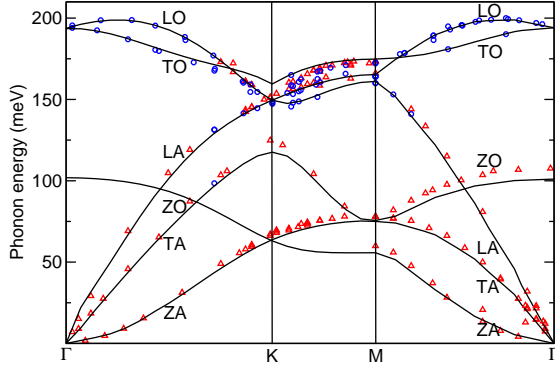


FIG. 3: (Color online) Our in-plane phonon dispersion of graphite together with a DFT calculation from Ref. 11 (solid lines). Same symbols as in Fig. 2 were used.

graphene sheets,¹⁰ however, this branch could not be detected, as the shear modes in graphene are forbidden in EELS. These contrasting results suggest that the crystalline quality of Ref. 8 was lower, softening the selection rules. This explains why some previous empirical models, relying on the then available EELS data, predicted a larger slope and consequently a crossing of the ZO and TA modes between the Γ and M points.

We measured for the first time the ZA and TA mode between the K and M points. Our results confirm predictions made by *ab-initio* calculations very well (Fig. 3), and are also well reproduced by our force-constant fit (Fig. 2). The trend of both branches crossing near the M point can be recognized.

The two optical phonons at the M point derived from the LO and LA branches are very close in frequency (< 4 meV), and we were not able to distinguish them clearly by symmetry. It appears, however, consistent with DFT calculations and the force constants fit in Sect. IV that the higher frequency has M_1^+ symmetry and the lower one M_4^- . As a consequence, the LO- and LA-derived branches cannot cross between the K and M point.

In Fig. 4 we show the low frequency phonon range along the $\Gamma - A$ direction, i.e., perpendicular to the in-plane direction. For comparison, we also present the INS data on highly oriented pyrolytic graphite from Ref. 7. They are in excellent agreement. The high-frequency phonon range is expected to show almost no dispersion along the $\Gamma - A$ direction.²⁰

Due to experimental reasons we were not able to record data points from the ZO branch along the $\Gamma - K - M$ direction. This branch has been measured in recent EELS experiments of Ref. 10. In general, the data of Ref. 10 agree well with ours, but at the K -point the ZO and ZA branches in Ref. 10 show a relatively large splitting of ≈ 10 meV. They cannot stem from

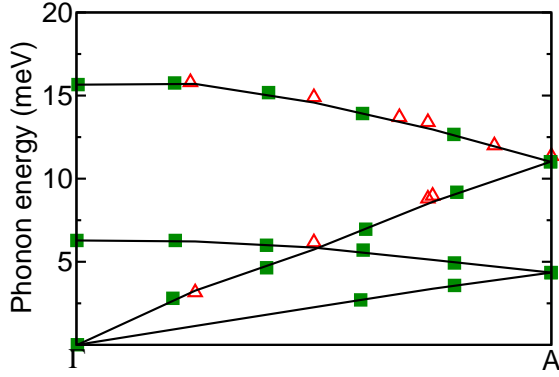


FIG. 4: (Color online) Phonon dispersion of graphite along the $\Gamma - A$ direction. Open triangles are present IXS data, full squares are neutron scattering data from Ref. 7. The lines are a guide to the eye.

the degenerate K_6 -phonon, but could possibly represent the out-of-phase modes of the graphite planes. On the other hand, in DFT calculations of graphite²⁰ this splitting seems much smaller than indicated by the EELS data.

Regarding the phonon modes specific for graphite with more than one layer, we find the low-energy out-of-phase modes near the Γ point. These are indicated by the dashed line in Fig. 2. We measured two out-of-phase ZO' phonons in the $\Gamma - M$ direction, with energies 13.6 meV and 23.3 meV at 0.16 of the $\Gamma - M$ distance and at 0.4 $\Gamma - M$, respectively. A quadratic extrapolation leads to a value of 12.5 meV at the Γ point, in agreement with 15.7 meV from neutron scattering data.⁷

The optical-phonon frequencies at the high-symmetry points from our experiment are summarized in Figs. 6, 7, and 8 together with the displacement patterns obtained by the force-constants calculations in Sect. IV. The acoustic phonon branches near the Γ point give information on the elasticity of graphite, which will be reported elsewhere.²⁵

IV. FORCE CONSTANTS CALCULATIONS

Phonon dispersion relations are often predicted from *ab-initio* DFT or from empirical force-constants (FC) calculations. Empirical force-constants models in graphite have so far included up to 4th-nearest neighbors, in order to reproduce the overbending of the optical branch near the Γ point.^{26,27} In the case of graphite, besides the details regarding the frequency values, both methods show differences in the shape of phonon branches, e.g., the position of the crossing of the ZO and TA modes near the M point. While in FC calculations a crossing of the ZO and TA branches between the Γ and M points is predicted, it is found in *ab-initio* results to take place between K and M . This probably stems from a fit to the only available TA mode from EELS experiments in Ref. 8, as our force-constants fit will show later (e.g. see Ref.27).

Further differences between force-constants and *ab-initio* DFT calculations are found regarding the LA and LO branches near the M point: In DFT results, the LO-derived

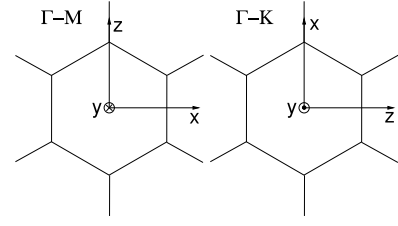


FIG. 5: Coordinate system for the point group C_{2v} of $\Gamma - M$ and $\Gamma - K$ drawn in real space. z points in the direction of the principal rotational axis.

phonon branch is higher than the LA phonon at the M -point, and, as a result, the two branches do not cross between M and K ; *vice versa* in most predictions by empirical force constants.

Discrepancies with the experimental data are found for both models for the TO-derived branch at the K point, except for Ref. 28. In this context we want to emphasize the importance of the K -point, when performing DFT calculations. The atomic forces in graphite are long ranged. Therefore, when using the finite-differences approach and DFT^{11,22,23} only the phonons commensurate with the supercell are calculated correctly. In linear-response calculations, on the other hand, the implementation of the K -point can be more easily achieved,^{12,20} however, the dynamical matrix at the K -point should be explicitly calculated and not be simply interpolated.

TABLE I: Symmetry relations between space group and molecular notation for the space group $P6_3/mmc$ and the point group D_{6h} . The corresponding coordinate system for C_{2v} is shown in Fig. 5.

Γ	D_{6h}	K	D_{3h}	M	D_{2h}	T, Σ	C_{2v}
Γ_2^-	A_{2u}	K_1	A'_1	M_1^+	A_{1g}	T_1, Σ_1	A_1
Γ_4^+	B_{2g}	K_2	A'_2	M_2^+	B_{1g}	T_2, Σ_2	A_2
Γ_6^-	E_{1u}	K_5	E'	M_2^-	B_{1u}	T_3, Σ_3	B_1
Γ_5^+	E_{2g}	K_6	E''	M_3^+	B_{2g}	T_4, Σ_4	B_2
				M_3^-	B_{2u}		
				M_4^-	B_{3u}		

A. Fitting procedure

To obtain the optimal fit of the set of force constants to the experimental data, we applied a variable neighbor search (VNS) method of global optimization²⁹, using the simplex method³⁰ for the local optimization subroutine. Basically, this is the least squares procedure minimizing the average deviation $\Delta(\mathbf{f}) = \frac{1}{N^{\text{exp}}} \sqrt{\sum_i |\omega_i^{\text{exp}} - \omega_i(\mathbf{f})|^2}$ between the $N^{\text{exp}} = 96$ experimental values, ω_i^{exp} , and the corresponding calculated frequencies, $\omega_i(\mathbf{f})$, obtained by calculation with the trial values of the force constants $\mathbf{f} = (f_1, \dots, f_F)$. Due to symmetry, for each level of the 3 or 6 neighbor atoms the same triple of force constants can be used. We used stretching, out-of-plane and in-plane force constants f_i for each relevant pair of atoms.^{27,31} Here, the direction of stretching cor-

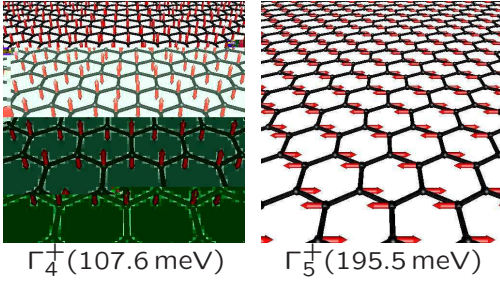


FIG. 6: (Color online) Optical eigenmodes of graphene at the Γ point from the force-constants calculation. The experimental frequency values are given in brackets; they are taken from the data recorded closest to the Γ point.

responds to the line that connects the center atom with the atom of appropriate level. The in-plane and out-of-plane directions are perpendicular to this line and lie in the graphene layer or perpendicular to it, respectively. After transforming the stretching and in-plane force constants to a global basis, one obtains the dynamical matrix. The level of the relevant neighbors has been gradually increased until the satisfactory agreement ($\Delta < 0.23\text{meV}$, with the greatest difference of $|\omega_i^{\text{exp}} - \omega_i(\mathbf{f})| \approx 8\text{ meV}$ for the LA branch in the $\Gamma - K$ region, nearby the K -point) has been eventually achieved with included neighbors of up to the fifth level. The fifth level contains 24 neighbors of each atom, as there are 3, 6, 3, 6, and 6 symmetrically positioned first to fifth neighbors, respectively, resulting in fifteen independent variational parameters f_i .

B. Force-constants results

The optimized values of the force constants parameters are presented in Table II. In Fig. 2 we show the phonon dispersion obtained from these force constants in comparison to the experimental data. The largest deviations between the calculation and the experiment occur for the optical phonon branches near the K point. This is probably due to the strong interaction of the near- K -point phonons with electrons near the Fermi level, which is not included in a force-constants model. Including more than 4th-nearest neighbors of atoms (i.e., fifteen independent parameters), however, gives a fairly good description of the local minimum of the TO-derived branch at the K point.

Moreover, although FC calculations including only fourth-nearest neighbors provide a considerably good average fit to the experimental data, they lead to permuted frequencies of the LO and LA-derived phonons at the M point (M_1^+ and M_4^-), and to a crossing of the LA and LO branches within the $K - M$ region ($K_5 - M_1^+$ and $K_5 - M_4^-$). Therefore, at least fifth-nearest neighbors are required for a good empirical description of the graphite phonon dispersion.

The eigenvectors of all optical phonons from our force-constants calculation at the high-symmetry points Γ , K , and M are drawn in Figs. 6, 7, and 8, respectively. They are in agreement with calculations from a molecular-based approach

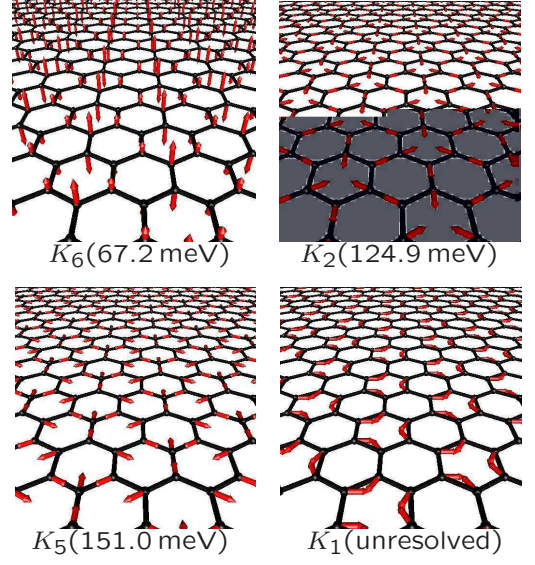


FIG. 7: (Color online) Eigenmodes of graphene at the K point. For the degenerate modes, only one choice per energy is given. Phonon energies given in brackets are the IXS experimental values. For the symmetry notation see Table I.

TABLE II: Force constants parameters for graphene, obtained from a fit to the experimental data, in $\text{eV}/\text{\AA}^2$.

Neighbor level	Stretching	Out of plane	In plane
1	25.880	6.183	8.420
2	4.037	-0.492	-3.044
3	-3.016	0.516	3.948
4	0.564	-0.521	0.129
5	1.035	0.110	0.166

of Ref. 28. For the degenerate modes, we show only one choice per energy; the remaining eigenvectors can be obtained by the symmetry-group projectors.

Often in literature the molecular notation for the symmetry groups is used. Therefore, Table I shows the relation between the spacegroup notation of $P6_3/mmc$ and the molecular notation at the high-symmetry points Γ , K , and M , and the lines $\Gamma - K - M$ (T) and $\Gamma - M$ (Σ). The eigenvectors will help to choose the sample orientation in future IXS experiments. The scattering cross section is zero, if the direction of the atomic displacements and the momentum transfer in the scattering process enclose an angle of 90° .

The above force constants parameters can in principle be used to calculate the phonon dispersion of carbon nanotubes, in particular for chiral nanotubes with a large number of atoms in the unit cell that require large computational effort, when calculated with first-principle methods. The existence of a

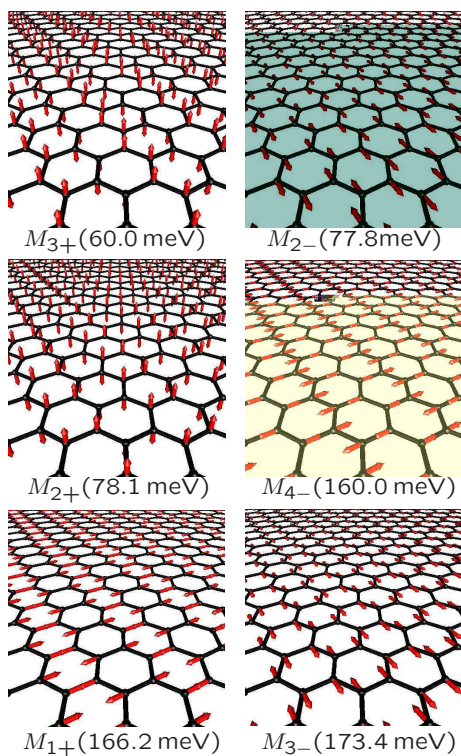


FIG. 8: (Color online) Eigenmodes of graphene at the M point (from lower to higher frequencies). Phonon energies given in brackets are the IXS experimental values. For the symmetry notation see Table I.

fourth acoustic mode (pure rotation of the tube about its axis) and the finite frequency of the radial breathing mode have to be taken into account, see Refs. 31,32,33. In addition, the different bond angles and lengths between the carbon atoms on the cylinder surface depending on the chiral index must be included. We expect that such an approach based on

the empirical force constants of graphite will give an overall good description of the phonon bands of carbon nanotubes. In metallic nanotubes, however, the coupling of the Γ -point and K -point phonons to the electronic system will lead to different results for those modes, see for instance the Kohn anomalies and the frequency drop of the LO phonon in metallic nanotubes.^{12,23,34} Therefore, where the phonon dispersion is modified due to strong interactions between the phonons and the electrons, a force-constants model might only give an empirical description of the phonon bands, but should be tested by DFT calculations which take electron-phonon coupling into account.

V. SUMMARY

In summary, we presented the full in-plane phonon dispersion of graphite determined by inelastic x-ray scattering. The overall shape of the phonon bands confirms previous *ab-initio* DFT calculations, if special care is taken for the highest optical phonons near the K point. We showed that by including fifth-nearest neighbors, the phonon bands can be well described within a force-constants model. Previous empirical models predicted only parts of the phonon dispersion correctly, since experimental data in the $K - M$ region had been missing. The new force constants will also improve the models of the phonon dispersion in carbon nanotubes.

VI. ACKNOWLEDGMENTS

We would like to thank M. Dražić for sharing his results prior to publication. We thank A.V. Tamashauský for the rare single crystals of graphite. J.M. acknowledges support from the Alexander-von-Humboldt foundation. This work was supported in part by the ESRF.

* Electronic address: marcel@physik.tu-berlin.de

† present address: Departments of Electrical Engineering and Physics, Columbia University, New York NY 10027, USA

¹ K. S. Novoselov, A. K. Geim, S. V. Morozov, D. Jiang, Y. Zhang, S. V. Dubonos, I. V. Grigorieva, and A. A. Firsov, *Science* **306**, 666 (2004).

² Y. Zhang, Y.-W. Tan, H. L. Stormer, and P. Kim, *Nature* **438**, 201 (2005).

³ S. Reich, C. Thomsen, and J. Maultzsch, *Carbon Nanotubes: Basic Concepts and Physical Properties* (Wiley-VCH, Berlin, 2004).

⁴ C. Thomsen and S. Reich, in *Light Scattering in Solids IX*, edited by M. Cardona and R. Merlin (Springer, Heidelberg, 2007), vol. 108 of *Topics in Applied Physics*, chap. 3.

⁵ J.-Y. Park, S. Rosenblatt, Y. Yaish, V. Sazanov, H. Üstünel, S. Braig, T. A. Arias, P. W. Brouwer, and P. L. McEuen, *Nano Lett.* **4**, 517 (2004).

⁶ M. Lazzeri and F. Mauri, *Phys. Rev. B* **73**, 165419 (2006).

⁷ R. Nicklow, N. Wakabayashi, and H. G. Smith, *Phys. Rev. B* **5**, 4951 (1972).

⁸ C. Oshima, T. Aizawa, R. Souda, Y. Ishizawa, and Y. Sumiyoshi,

Solid State Commun. **65**, 1601 (1988).

⁹ S. Siebentritt, R. Pies, K.-H. Rieder, and A. M. Shikin, *Phys. Rev. B* **55**, 7297 (1997).

¹⁰ H. Yanagisawa, T. Tanaka, Y. Ishida, M. Matsue, E. Rokuta, S. Otani, and C. Oshima, *Surf. Interface Anal.* **37**, 133 (2005).

¹¹ J. Maultzsch, S. Reich, C. Thomsen, H. Requardt, and P. Ordejón, *Phys. Rev. Lett.* **92**, 075501 (2004).

¹² S. Piscanec, M. Lazzeri, F. Mauri, A. C. Ferrari, and J. Robertson, *Phys. Rev. Lett.* **93**, 185503 (2004).

¹³ E. Burkel, *Rep. Prog. Phys.* **63**, 171 (2000).

¹⁴ M. Krisch and F. Sette, in *Light Scattering in Solids IX*, edited by M. Cardona and R. Merlin (Springer, Berlin, 2007), vol. 108 of *Topics in Applied Physics*.

¹⁵ P. Trucano and R. Chen, *Nature* **258**, 136 (1975).

¹⁶ A. K. Kirov, M. I. Aroyo, and J. M. Perez-Mato, *Journal of Applied Crystallography* **36**, 1085 (2003), see also the Bilbao crystallographic server, <http://www.cryst.ehu.es>.

¹⁷ R. J. Nemanich and S. A. Solin, *Phys. Rev. B* **20**, 392 (1979).

¹⁸ T. Inui, Y. Tanabe, and Y. Onodera, *Group Theory and its Application in Physics* (Springer, Berlin, 1996).

- ¹⁹ S. Reich and C. Thomsen, *Phil. Trans. R. Soc. Lond. A* **362**, 2271 (2004).
- ²⁰ P. Pavone, R. Bauer, K. Karch, O. Schütt, S. Vent, W. Windl, D. Strauch, S. Baroni, and S. de Gironcoli, *Physica B* **219**, 439 (1996).
- ²¹ R. J. Nemanich, G. Lucovsky, and S. A. Solin, *Solid State Comm.* **23**, 117 (1977).
- ²² D. Sánchez-Portal, E. Artacho, J. M. Soler, A. Rubio, and P. Ordejón, *Phys. Rev. B* **59**, 12678 (1999).
- ²³ O. Dubay and G. Kresse, *Phys. Rev. B* **67**, 035401 (2003).
- ²⁴ J. Kulda, H. Kainzmaier, D. Strauch, B. Dorner, M. Lorenzen, and M. Krisch, *Phys. Rev. B* **66**, 241402(R) (2002).
- ²⁵ A. Bosak, M. Krisch, M. Mohr, J. Maultzsch, and C. Thomsen, *Phys. Rev. B* **75**, 153408 (2007).
- ²⁶ R. Al-Jishi and G. Dresselhaus, *Phys. Rev. B* **26**, 4514 (1982).
- ²⁷ R. A. Jishi, L. Venkataraman, M. S. Dresselhaus, and G. Dresselhaus, *Chem. Phys. Lett.* **209**, 77 (1993).
- ²⁸ C. Mapelli, C. Castiglioni, G. Zerbi, and K. Müllen, *Phys. Rev. B* **60**, 12710 (1999).
- ²⁹ M. Dražić, C. Lavor, N. Maculan, and N. Mladenović, *Journal of Operational Research* (to appear 2006).
- ³⁰ W. Press, B. P. Flannery, S. A. Teukolsky, and W. T. Vetterling, *Numerical Recipes* (Cambridge University Press, Cambridge, 1986).
- ³¹ E. Dobardžić, I. Milošević, B. Nikolić, T. Vuković, and M. Damnjanović, *Phys. Rev. B* **68**, 045408 (2003).
- ³² R. Saito, T. Takeya, T. Kimura, G. Dresselhaus, and M. S. Dresselhaus, *Phys. Rev. B* **57**, 4145 (1998).
- ³³ J. Maultzsch, S. Reich, C. Thomsen, E. Dobardžić, I. Milošević, and M. Damnjanović, *Solid State Comm.* **121**, 471 (2002).
- ³⁴ S. Piscanec, M. Lazzeri, J. Robertson, A. C. Ferrari, and F. Mauri, *Phys. Rev. B* **75**, 035427 (2007).